EXTRACTION OF SLOW MUONS GENERATED NEAR TARGET†

KOSAI TANABE‡

Physics Department, Yale University, New Haven, Connecticut, USA

The behaviour of the slow muons generated from the pion decay near the primary target is investigated in great detail. The calculations are based on the recently available pion production cross sections, which include measurements at large production angles and low momenta. The characteristics of the available muon flux are derived by evaluating the intensity distribution in momentum space, muon polarization, and integrated flux intensity for various parameters of an intentionally misaligned channel.

Applying the above results we investigate possible methods of transport. Evaluations of the beam intensity and average polarization are carried out for some simple systems. The result implies that the expected output intensity is comparable to that from an elaborate stopped muon channel of the standard type.

1. INTRODUCTION

Recent developments in elementary particle physics, nuclear physics, and atomic physics have indicated the need for intense muon beams.[1,2,3] Several such muon channels[4,5,6,7] are already in use, or under construction.[8,9] The method of muon collection and transport in all these channels is based on the principle whereby an intense pion flux is guided through one portion of the channel, and the major part of the muon beam is generated via decay. The residual pions are separated from muons at a later stage. There are, of course, some differences in the tunings of the channels, target positions, transport methods, and in the separation of the surviving pions. In this type of channel muons generated upstream of the entrance to the system contribute little to the output flux.

Experience in experimental meson physics,[10] and calculations relevant to the estimation of the muon flux in the recent design study of a stopped muon channel[8] suggest the existence of a very significant slow muon flux, or 'cloud' generated from the decays of very low energy pions near the primary target.

The present investigation is also motivated by the available data[11] for the production cross section of charged pions at large production angles and low momenta. These show interesting behaviour from our point of view. Pion production changes slowly with increasing production angle ($\lesssim 90°$) for

momenta less than 400 MeV/c; and it can be even larger at 90° than at smaller angles, for some momenta ($\lesssim 200$ MeV/c). Therefore the muon distribution is expected to be spread widely in production angle as well as in momentum space.

This fact suggests another possibility for a high intensity, low momentum muon beam which would be feasible for stopped muon experiments, provided that a suitable method of collection and transport can be found. If this could be achieved with simple and inexpensive magnet systems, the muon cloud channel would be extremely practicable.

The purpose of present paper is dual: first, we study the characteristics of the muon flux in great detail, and secondly consider the possible extraction schemes. The calculations in the present paper are based on the experimental pion production cross sections[11] measured by the group of the Los Alamos Scientific Laboratory and the values obtained by extrapolating those data to the low momentum region ($\lesssim 80$ MeV/c) via the empirical formula presented in Sec. 2. No approximation is made for the decay kinematics. Through Sec. 4 all the properties of the muon clouds will be computed neglecting the primary target size in comparison with the distance to the virtual entrance of the channel, and with its aperture. Our principal results will not be much affected even if account is taken of the actual target size. However, it will be considered to design the channel in Sec. 5. All the calculations have been carried out numerically on the IBM 7094 computer at Yale University.

In Sec. 2 the characteristics of the muon cloud in momentum space at a given spatial point will be

‡ Present Address: Department of Physics, Saitama University, Urawa, Saitama-ken, Japan.

investigated by evaluating the distribution and the polarization. In Sec. 3 the broadness of the muon distribution in momentum space will be stressed by comparing the integrated distributions expected at various misalignment angles. The average polarization will also be calculated.

In Sec. 4 from the extraction point of view the characteristics of the muon flux will be studied at the entrance to a transport system, with finite aperture size and with the assumed limits on the acceptance angles.

In Sec. 5 possible designs of extraction channels will be considered by evaluating the output beam intensity. In Sec. 6 our results will be summarized and those implications will be discussed.

2. MUON DISTRIBUTION AND POLARIZATION IN MOMENTUM SPACE

The momentum space distribution for muons generated in large angle decays differs considerably from that appropriate to pions. The properties of those muon clouds will be investigated for low momenta ($\lesssim 150$ MeV/c), for which this characteristic is especially true. Since a large portion of the muon cloud distribution overlaps spatially with pion flux, it will be accepted by the usual muon channel, which has large acceptance both in physical aperture and momentum direction. It is lost, however, at the channel wall or removed along with the pions at the analysing section of the channel. It should be possible, however, to extract muon clouds, if the momentum space distribution is wide enough.

Since the pion production cross section at the very low momentum region ($\lesssim 80$ MeV/c) is unknown, it is to be extrapolated from the measured cross sections at higher momenta. For this purpose the following simple dependence† of the differential production cross section on pion momentum is assumed:

$$\partial^3 \sigma_\pi / \partial p_\pi \, \partial \cos\theta \, \partial\phi \propto p_\pi^2 \cdot \exp\left[-p_\pi(1+\theta/\beta)/\alpha\right]$$
$$\cdot (1-\theta/\pi)(1+\theta/\gamma) \cdot \theta/\sin\theta, \quad (1)$$

where the numerical values of the three parameters

$$\alpha = 139.5 \text{ MeV/c}, \quad \beta = 0.863, \text{ and } \gamma = 0.0802 \quad (2)$$

† Similar exponential dependence is used in Ref. 13.

are derived from the experimental cross sections[11]‡ at large angles ($\leq 90°$), for 747-MeV protons on a copper target.

Adjusting the value of the numerical constant multiplying the right-hand side of Eq. (1) reproduces the π^- production cross section to ± 10 per cent in the relevant regions of momenta. The following calculations are carried out exclusively for the case of π^- and μ^-. However, the intensities for π^+ and μ^+ will be crudely inferred from the corresponding π^- results by multiplying these by three, since the π^+ yield at low momenta ($\lesssim 150$ MeV/c) and large angles ($45° - 90°$) is roughly from two to four times as large as the π^- yield.

Throughout the present paper the following values are assumed fixed:

Proton beam intensity: $I = 1 \ \mu$A
Initial kinetic energy = 750 MeV
Copper target thickness: $t = 3.4$ cm (corresponding to 50-MeV kinetic energy loss).

The pion intensity per unit momentum, and per unit solid angle $\partial^2 N_\pi / \partial p_\pi \, \partial\Omega_\pi$ is related to the differential production cross section $\partial^2 \sigma_\pi / \partial p_\pi \, \partial\Omega_\pi$ (μb · (MeV/c · sr)$^{-1}$) by

$$\partial^2 N_\pi / \partial p_\pi \, \partial\Omega_\pi = N \cdot \partial^2 \sigma_\pi / \partial p_\pi \, \partial\Omega_\pi, \quad (3)$$

where the numerical constant N is given in terms of

Avogadro number: $A = 6.023 \times 10^{23} \text{ mole}^{-1}$
Atomic mole weight of copper: $M = 63.54 \text{ g·mole}^{-1}$
Density of copper: $\rho = 8.96 \text{ g·cm}^{-3}$
Unit charge: $e = 1.60 \times 10^{-19}$ Coulomb

Thus:

$$N = (A\rho/M) \cdot (I/e) \cdot t = 1.80 \times 10^6 \text{ sec}^{-1} \quad (4)$$

The longitudinal polarization P_μ of muon in its rest frame is given by

$$P_\mu = \cos\psi_{\text{pol}} = \frac{e}{|e|} \frac{(1-\beta_\mu)E_\pi - E_\mu}{\beta_\mu p_\mu}, \quad (5)$$

where ψ_{pol} is the angle of the spin direction measured from the direction of laboratory momentum, E_π and E_μ are the laboratory energies of pion and

‡ The low energy pion production cross sections by 725 and 600 MeV protons on various nuclei, observed at the production angle less than 21.5°, are given in Ref. 12.
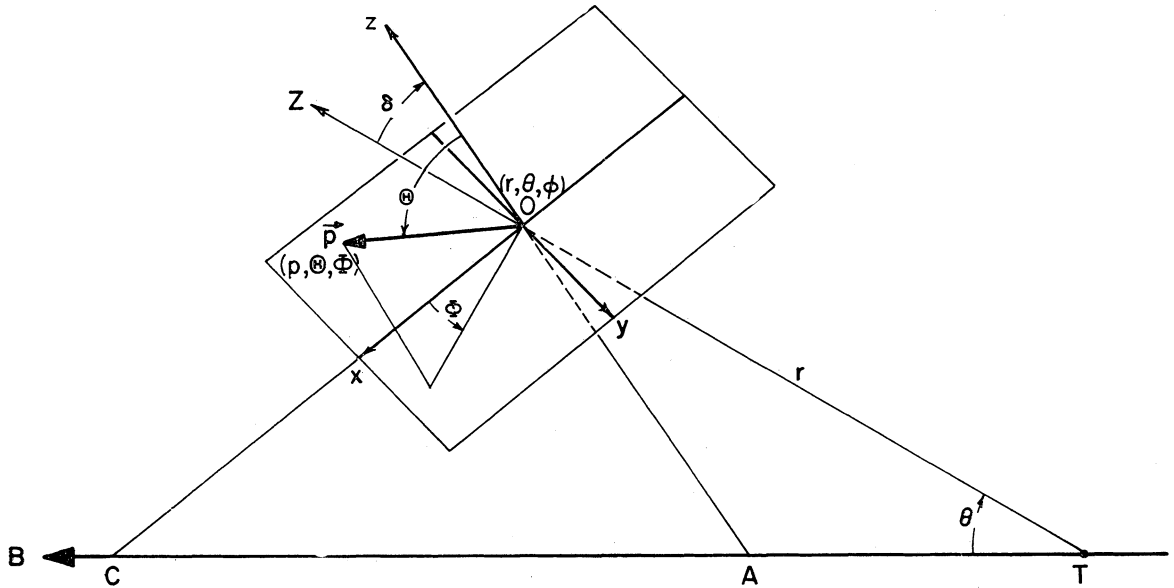
FIG. 1. Definitions of coordinates.

muon respectively, p_μ the muon laboratory momentum, and $\beta_\mu = (m_\pi{}^2 - m_\mu{}^2)/(m_\pi{}^2 + m_\mu{}^2)$.

In order to describe the distribution at a given spatial point the following coordinates are defined (see Fig. 1). The flux is examined at the reference point O which is specified by the coordinates (r, θ, ϕ) relative to the center of the point target T, where r is the distance from the point T, θ the polar angle, or production angle measured from the direction of the proton beam TB, and ϕ the azimuthal angle.

The flux is assumed to be measured through the plane, or flat window whose normal direction, Oz, is specified by the deviation angle δ, measured from the direction TOZ. The misalignment of the plane is specified by this quantity δ. Hereafter the axes Oz, OZ and the beam line TB are supposed to be coplanar. Further, the deviation angle δ is defined to be positive (negative), when the point A, where the axis Oz intersects the beam line, is downstream (upstream) of the target T.

The Cartesian coordinate system O-xyz is defined, in which the xy-plane defines the window surface and the x-axis intersects the beam line at point C. The momentum vector $\mathbf{p}$ is described by the polar coordinates (p, Θ, Φ).

In momentum space the muon distribution at a given spatial point is expressed by the quantity

$\partial^3 N_\mu / \partial p_\mu \, \partial \Omega \, \partial s$, which is a function of the momentum $\mathbf{p}_\mu(p_\mu, \Theta, \Phi)$, the position specified by the distance r and the production angle θ, and the deviation angle δ. Here ds stands for the element of the area dxdy defined in the xy-plane. The solid angle element dΩ defined in momentum space is given by d$(-\cos \Theta)$dΦ.

Typical examples of the calculated differential distributions expected at the windows for deviation angles $\delta = 0°$ and $5°$ are plotted in Figs. 2(a) and 2(b), respectively. As for the distributions at the window without misalignment at a production angle $\theta = 90°$ and a distance $r = 50$ cm, there appears to be no significant structure with respect to the azimuthal angle Φ, for the nonzero values of Θ at any momentum greater than 25 MeV/c. This is because the π^- production cross section varies little with the production angle at about 90°. This fact holds also for the distribution at smaller production angles ($\gtrsim 45°$).

For muons with momenta less than 100 MeV/c and Θ less than 10°, the number of muons increases with increasing momentum. This comes about because of the rapidly increasing number of muons produced in forward pion decays. The pion flux increases with momentum up to about 120 MeV/c.

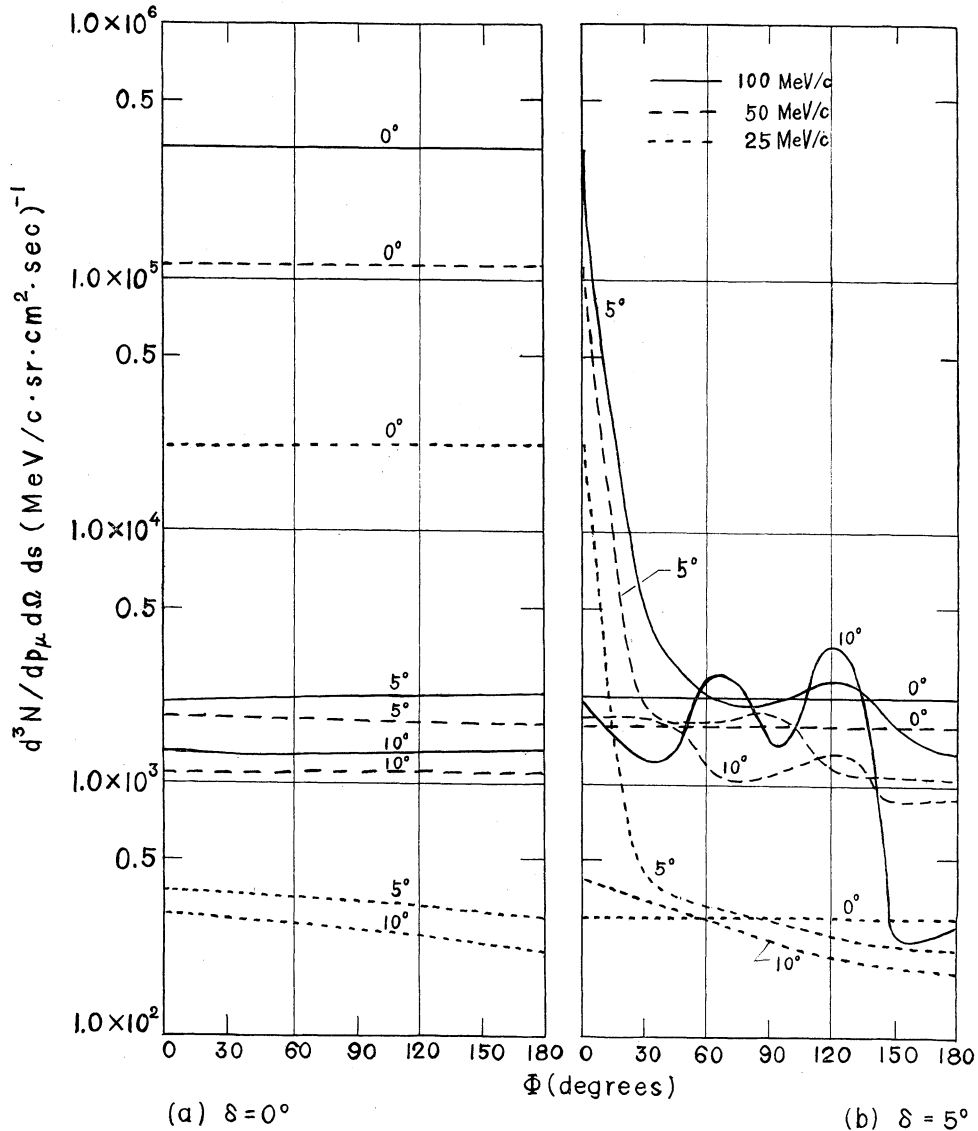The larger the muon momentum, the more rapidly distribution of muons increases with

FIG. 2. The muon distribution in momentum space at the production angle of 90° and the distance of 50 cm. The abscissa is the azimuthal angle Φ, and the ordinate is the number of muons per unit volume of momentum space, per unit time, and per unit area at the center of the misaligned window with the deviation angle of 0°, or 5°. The distributions are given for momenta of 100 MeV/c (solid curves), 50 MeV/c (dashed curves) and 25 MeV/c (dotted curves), at various polar angles Θ of the momentum vector $\mathbf{p}_\mu$, which are assigned to the curves.

decreasing Θ, as expected from kinematics. For instance, the distribution for a momentum of 100 MeV/c at $\Theta = 0°$ is 300 times greater than at $\Theta = 10°$, while the distribution for a momentum of 50 MeV/c at $\Theta = 0°$ is 100 times greater than at $\Theta = 10°$.

When the distribution is observed with $\delta = 5°$, as shown in Fig. 2(b), there appears a forward peak

(for small Φ) at $\Theta = 5°$, which corresponds to the distribution at $\delta = 0°$ and $\Theta = 0°$ shown in Fig. 2(a).

There are some complicated, but unimportant structures which are closely related to the details of the pion distribution. However, comparing the two diagrams we can infer that the reduction in integrated muon flux at finite δ need not be substantial. The apparent large difference in the

distributions at $\Theta = 0°$ is not significant when integrated, because of the correspondingly small phase-space volume. This fact will be confirmed by the explicit calculations in the next section.

The polarization of muons for $\theta = 90°$ and $r = 50$ cm is plotted as the function of the momentum $\mathbf{p}_\mu(p_\mu, \Theta, \Phi)$ for $\delta = 0°$ and $\delta = 5°$ in Figs. 3(a) and 3(b), respectively. The sign of the polarization is positive for μ^- produced forward in the rest frame of π^-. At low momenta (30 MeV/c − 50 MeV/c), the polarization is negative due to the large admixture of the muons from backward decays in the pion rest frame, but emitted forward in the laboratory frame.
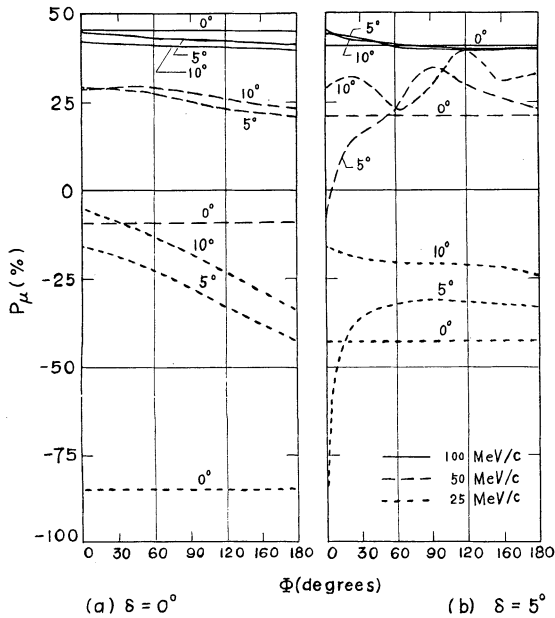

FIG. 3. The muon polarization in momentum space at the production angle of 90° and the distance of 50 cm. The abscissa is the azimuthal angle Φ, and the ordinate is the polarization. The polarizations are given for muon momenta of 100 MeV/c (solid curves), 50 MeV/c (dashed curves) and 25 MeV/c (dotted curves), at various polar angles Θ of the momentum vector $\mathbf{p}_\mu$, which are assigned to the curves.

At momenta less than 30 MeV/c no muon is produced forward in the pion rest frame, so that the polarization is more negative. The positive values of the polarization at $\Phi = 0°$ and $\Theta = 5°$ in Fig. 3(b) correspond to those at $\Theta = 0°$ in Fig. 3(a).

As a whole the polarization is small except at very low momenta.

3. EXPECTED FLUX AND POLARIZATION

In order to investigate the behaviour of the muon cloud flux the distribution is integrated over a certain extent of the solid angle in momentum space. For a maximum value $\Theta_{max} = 6°$ of the polar angle around the normal to the virtual observation window the muon flux intensity at the center of the window is evaluated by

$$\partial^2 N_\mu/\partial p_\mu \partial s$$
$$= \int_0^{\Theta_{max}} d\Theta \sin\Theta \int_0^\pi d\Phi \, \partial^3 N_\mu/\partial s \, \partial p_\mu \, \partial\Omega. \quad (6)$$

The average polarization is also evaluated.

In Figs. 4(a) and 4(b) the expected muon flux intensity, and the average polarization at $r = 50$ cm, and at $\theta = 45°$ and $\theta = 90°$ are plotted as functions of p_μ and δ. In Figs. 5(a) and 5(b) the same quantities are plotted for $r = 100$ cm. As long as the target size is negligibly small, the pion flux intensity is constant for the δ less than Θ_{max}. The pion flux intensities plotted in Figs. 5(a) and 5(b) are given in this sense and vanish for $\delta > \Theta_{max}$.

There is essentially no difference in muon spectra and polarizations shown in Figs. 4 and 5. The muon intensities at $r = 100$ cm are less than those at $r = 50$ cm by at most a factor of two, while the factor is about four for the pion intensities. This holds for momenta between 25 MeV/c and 150 MeV/c. The muon intensities at $\theta = 45°$ are larger than those at $\theta = 90°$ by a factor of less than two.

The maximum flux intensity is dependent on δ, but is restricted to momenta between 75 MeV/c and 100 MeV/c, for a production angle of 90°.

It is remarkable that the dependence of the intensity upon the δ is very slight. The reduction in intensity is less than the factor of two at low momenta ($\lesssim 100$ MeV/c), even for a misalignment of the window of $\pm 10°$. We expect, therefore, that the momentum space distribution of the slow muons extends to a region which does not overlap the pion flux, whose distribution is simply determined by the geometrical position and the size of the target. This characteristic of the muon cloud will be further investigated in the next section.
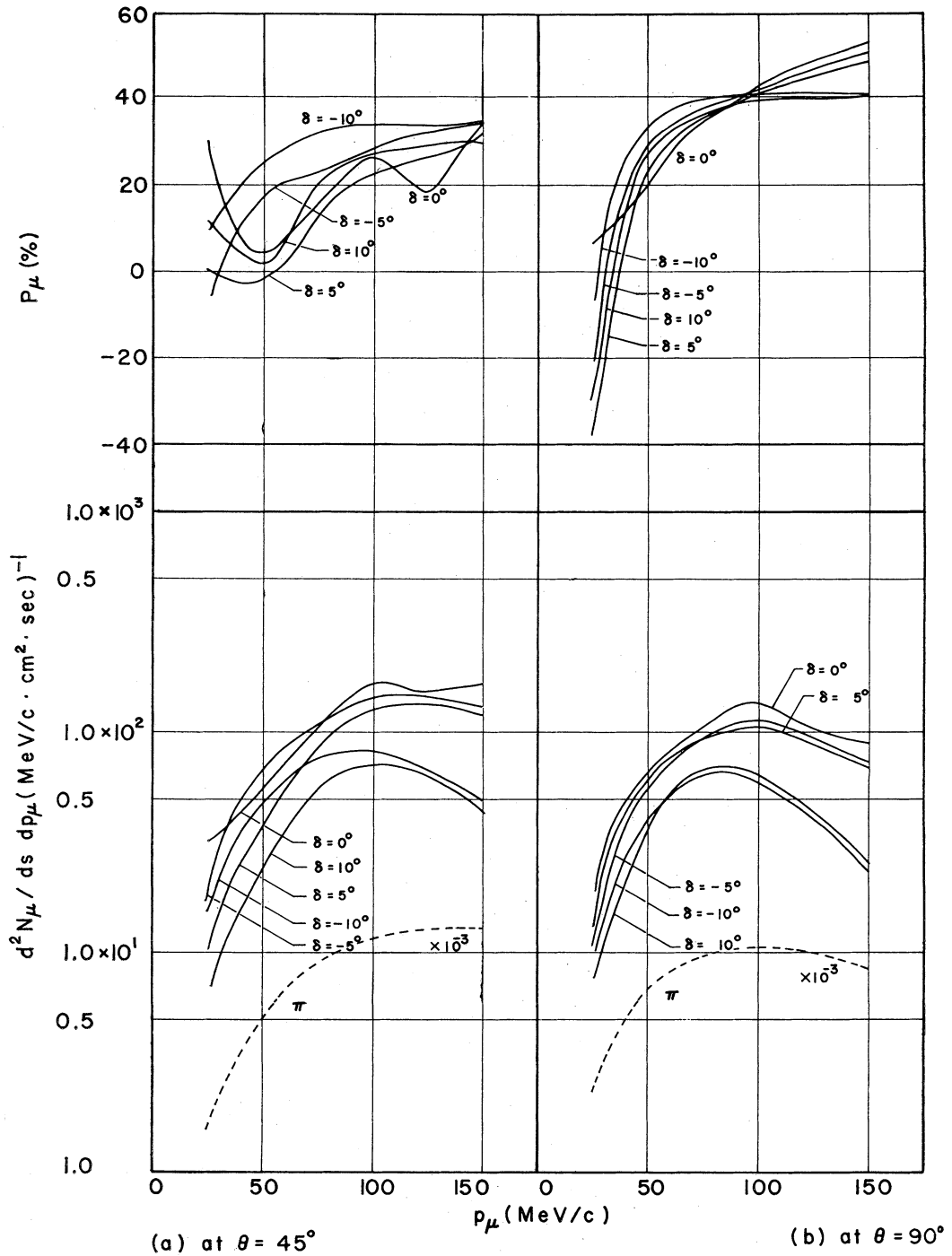
FIG. 4. Flux intensity and average polarization expected at the center of the misaligned window at the distance of 50 cm. The muon intensity is evaluated by integrating the distribution in momentum space up to 6° with respect to the polar angle Θ. The value of the deviation angle δ is indicated in the diagrams. The pion intensity is given by the broken line, which is converted to the correct one by multiplying by the factor 10^3 as indicated in the diagrams.
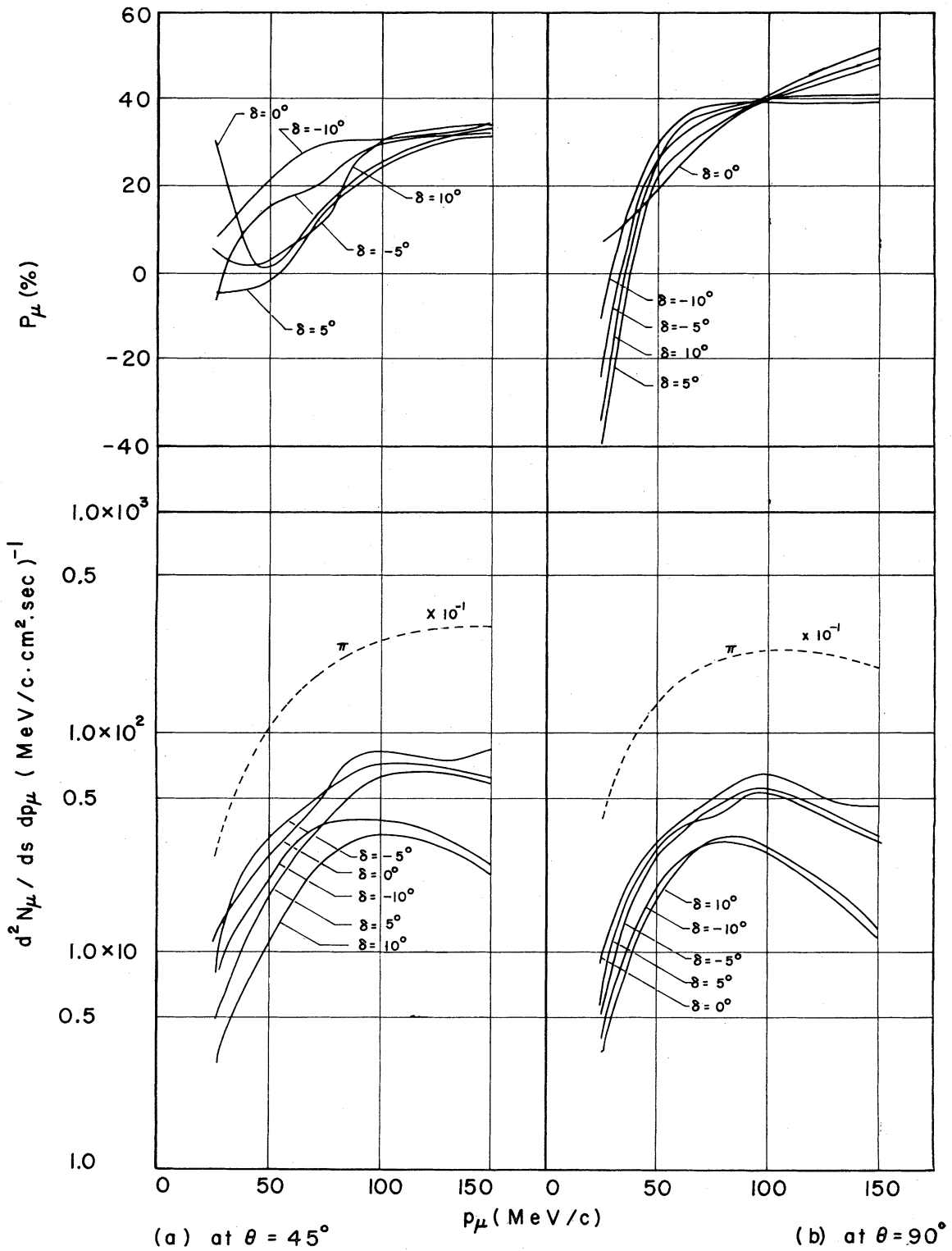
FIG. 5. Flux intensity and average polarization expected at the center of the misaligned window at the distance of 100 cm. The notation is the same as in Fig. 4.

A 5

The dependence of the angle-averaged polarization on momentum is more marked at $\theta = 90°$ than at $\theta = 45°$. The backward–forward ratio R_{BF} is defined by the number of muons from the backward decays divided by one from the forward decays. In Fig. 6 it is plotted at various production angles and deviation angles. Since it differs little from unity for momenta between 50 MeV/c and 100 MeV/c, the average polarization is small in this momentum range.
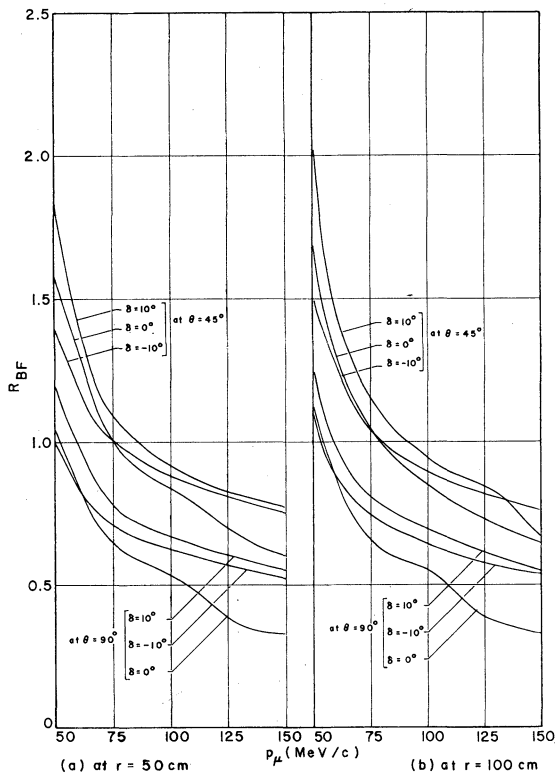

FIG. 6. Backward–forward ratio. The production angle θ and the deviation angle δ are indicated in the diagrams.

In summary, the flux intensity of muon clouds does not critically depend on the production angle, and it is reduced less than the pion intensity with increasing distance. The broadness of the spectrum in the momentum direction is described by its dependence on the deviation angle. This small dependence strongly suggests the possibility of collecting muons by misaligning the entrance to the channel to admit fewer pions. The expected

average value of the polarization will be less than 50 per cent for a reasonable acceptance, except for the very low momentum region ($\leqq 30$ MeV/c).

4. CHARACTERISTICS OF THE MUON AND PION FLUXES AT THE MISALIGNED ENTRANCE TO THE CHANNEL

In order to investigate the behaviour of the muon beam at the entrance to the channel we have to know the beam intensity, which is defined as the total flux intensity of muons passing through the entrance aperture. It is a function of the production angle θ, the distance r, and the deviation angle δ. When the finite size of the aperture is taken into consideration, the beam intensity is calculated by integrating the distribution, which is a function of coordinates (x, x', y, y'), over a limited phase-space volume. The muon beam intensities and the average polarizations expected at the entrance for various δ, at $\theta = 90°$, are plotted in Fig. 7(a) for $r = 50$ cm, and in Fig. 7(b) for $r = 100$ cm. Here, the size of the square aperture is 27.5 cm × 27.5 cm, and the limits of acceptance in momentum direction is $\pm 12.6°$ in both the x- and y-directions. It is recognized that at a given δ the muon spectrum has a maximum at a momentum greater than 100 MeV/c. For δ less than 5°, the muon intensity at $r = 100$ cm is higher than at $r = 50$ cm, while the pion intensity at $r = 100$ cm is much less than at $r = 50$ cm. The average polarization increases with increasing momentum, but it is still less than 40 per cent at 100 MeV/c.

In Fig. 8 the pi-mu ratio $R_{\pi\mu}$, which is defined as the number of pions divided by the number of muons, is plotted for various δ, for $r = 50$ cm and 100 cm. It is noticed that first, these ratios are much smaller at $r = 100$ cm than at $r = 50$ cm, and secondly, the minima are located at momenta between 65 MeV/c and 80 MeV/c. The ratio is not reduced with increasing δ. This is due to the fact that the assumed limits for the integration are large enough to admit many pions even at $\delta = 10°$.

The xx' (yy') phase-space distribution is calculated by integrating the distribution over the limited yy' (xx') phase-space volume. The typical examples of the xx' and yy' phase-space distributions are given in Figs. 9 and 10, respectively, for a
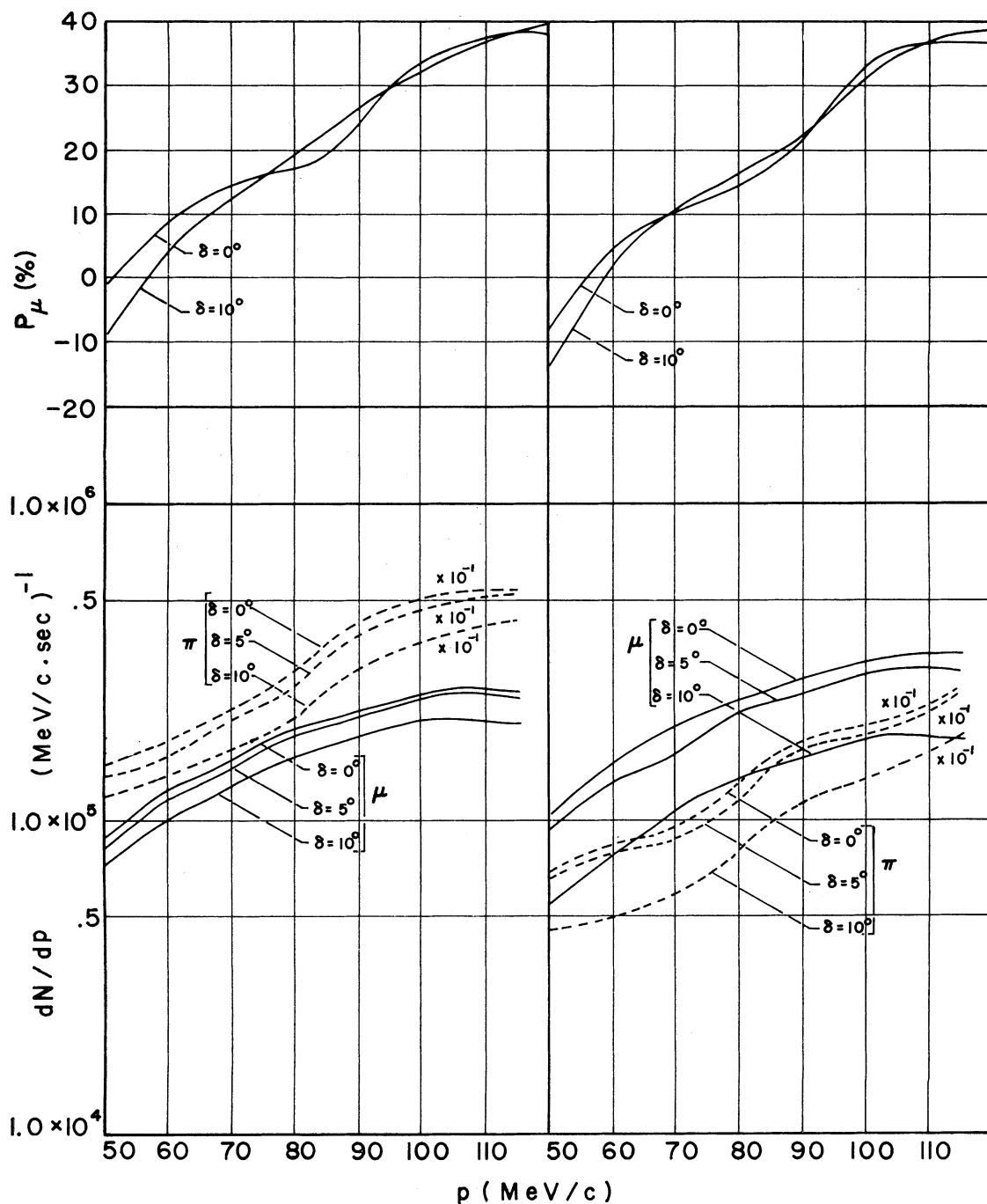
FIG. 7. Muon and pion spectra and average polarization expected at the misaligned window at the production angle of 90°. The deviation angle δ is indicated in the diagrams. The pion spectrum is given by the broken line, which is converted to the correct one by multiplying by the factor 10 as indicated in the diagrams. The window size is specified in the text.
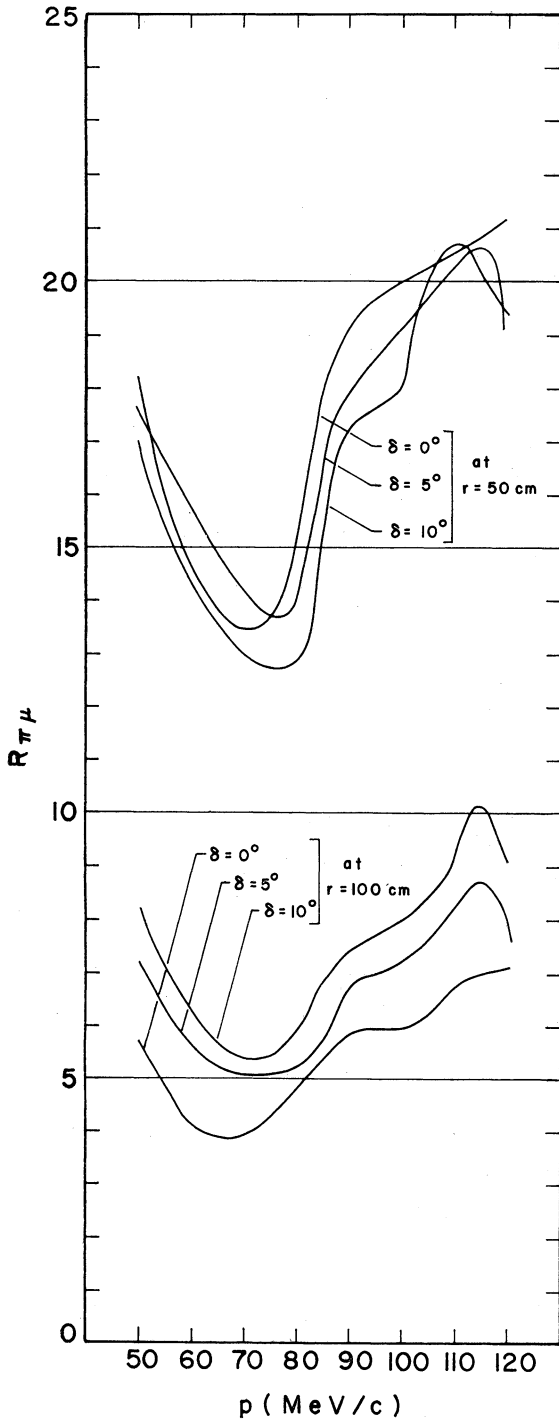
FIG. 8. Pi-mu ratio. The distance and the deviation angle are indicated in the diagram.

larger than that of muons, but the phase-space distribution of the pions is located by geometrical limits. The pion flux is obviously diverging for $\delta = 0°$, but with increasing δ this pion distribution is pushed toward the upper left in the xx' phase-space.

In Table I the average coordinates of the positions where accepted muons are generated are shown for momenta of 60 MeV/c and 100 MeV/c. It is inferred that most of such muons are generated about a point midway between the target and the entrance.

5. SOME CONSIDERATIONS ON POSSIBLE CHANNELS FOR EXTRACTION

In contrast to the usual muon channel the functions of the muon cloud channel are to collect slow muons, and at the same time to reduce the
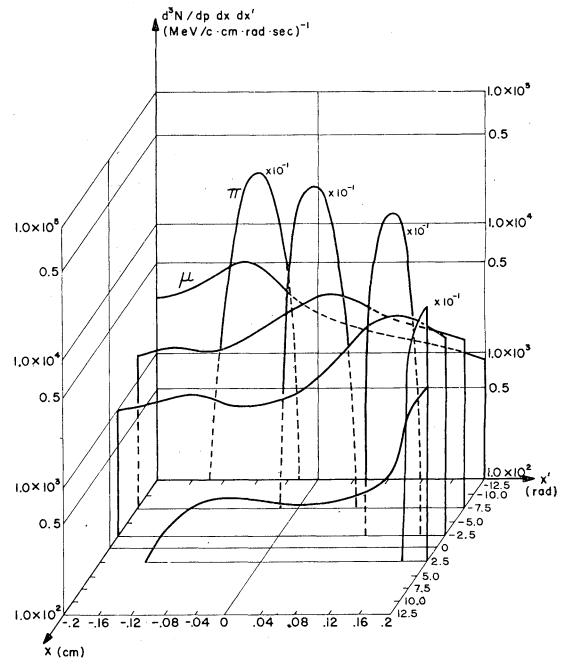

FIG. 9. Muon and pion distributions in the xx' phase-space. The distribution is given for the momentum of 75 MeV/c. The window is misaligned with the deviation angle of 10°, at the production angle of 90° and the distance of 50 cm. The width of the window and the limits of the angular acceptance in the y-direction are taken to be 27.5 cm and $\pm 12.6°$, respectively. As indicated in the diagram the factor 10 has to be multiplied to the value given by the curve for the pion distribution.

momentum of 75 MeV/c with $\delta = 10°$, $\theta = 90°$ and $r = 50$ cm. The total intensity of pions is much

$d^3N / dp\ dy\ dy'$
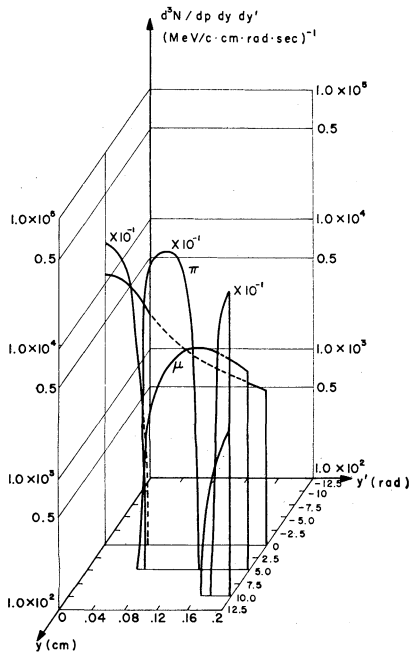$(MeV/c \cdot cm \cdot rad \cdot sec)^{-1}$

FIG. 10. Muon and pion distributions in the yy' phase-space. The distribution is given for the momentum of 75 MeV/c. The other half of the diagram for the negative y-axis is omitted because of the symmetry of the distribution with respect to the origin. The window is misaligned with the deviation angle of 10°, at the production angle of 90° and the distance of 50 cm. The width of the window and the limits of the angular acceptance in the x-direction are taken to be 27.5 cm and ±12.6°, respectively. As indicated in the diagram the factor 10 has to be multiplied to the value given by the curve for the pion distribution.

number of background pions. The simplest idea is to intentionally misalign the channel so that the target is shifted from the optical axis. Actually the fine adjustment of the deviation angle δ will be carried out by moving the target along the direction of the beam line. Then the incoming pions are blocked by the channel wall, or by an added stopper.

However, it may not be adequate to reject pions only by this geometrical misalignment. This is especially true for high momentum pions for which the produced muon distribution overlaps significantly the pion distribution. If we make the channel selective enough to make use of this simple method, then the loss of intensity will be substantial. Because of this problem we have to make use of a combination of this misalignment and a specific setup and tuning of the channel.

As a possible setup, let us consider the channel composed of a pair of quadrupole magnets with the square cross sections of half-aperture 13 cm and length 30 cm, two successive parallel faced dipole magnets with half-gap size 13 cm and length 75 cm each providing 45°-bend in opposite directions, and a pair of similar quadrupole magnets. A pion stopper with a vertical asymmetric slit is placed between the two dipoles. The whole system is schematically shown in Fig. 11. The names of the elements, the sizes of the magnets and drift spaces, and the bending angles are summarized in the first six columns of Table II.

The proton beam line is in the bending plane (xx' phase-space) of this channel. The total length from the point A of the channel entrance to point B of the channel exit is 575 cm. The entrance aperture is placed with a deviation angle of 10° at $\theta = 90°$ and $r = 50$ cm. This setup will be referred to hereafter as the horizontal channel.

Since there is a minimum pi-mu ratio at a momentum between 70 MeV/c and 80 MeV/c as seen in Fig. 8, the tuning of the whole system is adjusted for the momentum range from 70 MeV/c·

TABLE I

Average decay position. The average decay position is given in terms of the average coordinates $\bar{x}$, and $\bar{z}$. The channel entrance is placed at the production angle of 90°. The window size is specified in the text.

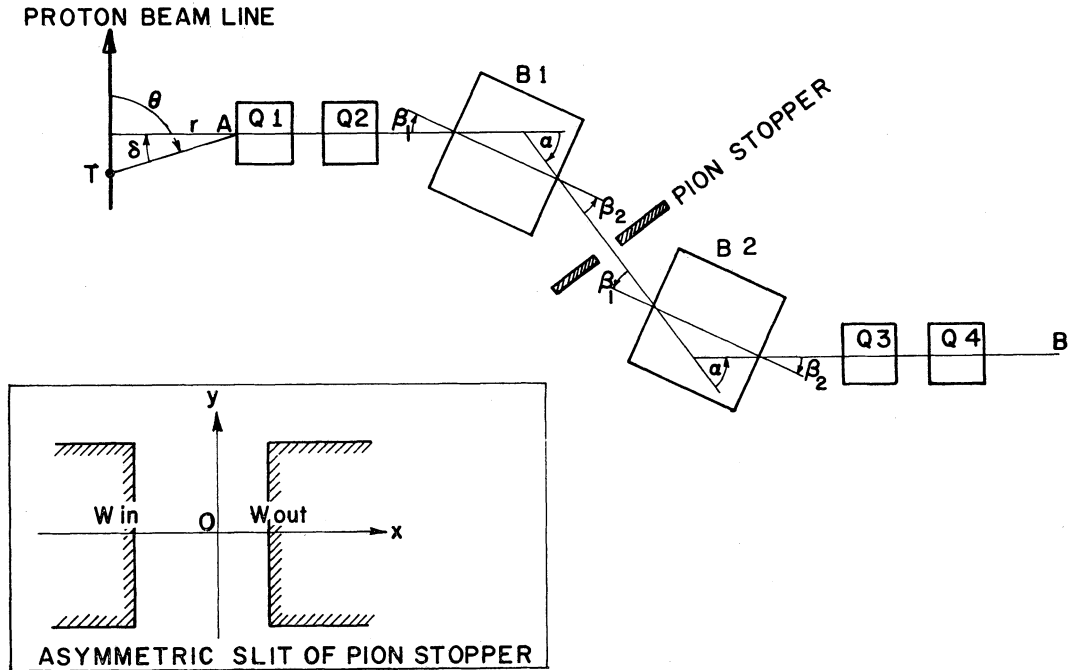| | | | Distance | 50 cm | | | 100 cm | | |
			Deviation angle	0°	5°	10°	0°	5°	10°
Momentum	60 MeV/c	$\bar{x}$		0 cm	−4.0 cm	−7.5 cm	0 cm	−5.1 cm	−10.6 cm
		$\bar{z}$		−25.2	−26.4	−25.9	−50.4	−49.3	−46.7
	100 MeV/c	$\bar{x}$		0	−3.9	−7.5	0	−5.1	−10.5
		$\bar{z}$		−25.4	−25.5	−25.0	−49.8	−48.7	−45.9

FIG. 11. Muon cloud channel. T: center of primary target; A: entrance point to the channel; B: exit point from the channel; α: bending angle; β_1 and β_2: angles of the pole face rotation. The coordinates W_{in} and W_{out} stand for the inside limits of the asymmetric slit of the pion stopper. The meanings of the parameters r, θ, and δ are defined in Fig. 1.

TABLE II

Parameters for channel elements. The arrangement of the quadrupoles ($Q1$, $Q2$, $Q3$ and $Q4$) and the dipoles ($B1$ and $B2$) is given by Fig. 11. 'Defocusing', or 'focusing' in the last column refers to the way of tuning seen in the x-direction.

Name of element	Length (cm)	Size of the element Half-width (cm)	Half-height (cm)	Bending angle α (degree)	β_1 and β_2 (degree)	Example of the tuning Field strength	Others
Q-pole ($Q1$)	35.0	13.0	13.0			0.219 kG/cm	defocusing
drift space	20.0	13.0	13.0				
Q-pole (Q2)	35.0	13.0	13.0			0.154 kG/cm	focusing
drift space	50.0	30.0	13.0				
D-pole ($B1$)	75.0	30.0	13.0	45.0	25.5	2.55 kG	central momentum = 75.0 MeV/c
drift space	45.0	30.0	13.0				
pion stopper	5.0						$W_{in} = -13.0$ cm, $W_{out} = 4.0$ cm
drift space	45.0	30.0	13.0				
D-pole ($B2$)	75.0	30.0	13.0	45.0	25.5	2.81 kG	central momentum = 82.5 MeV/c
drift space	50.0	30.0	13.0				
Q-pole ($Q3$)	35.0	13.0	13.0			0.114 kG/cm	focusing
drift space	20.0	13.0	13.0				
Q-pole ($Q4$)	35.0	13.0	13.0			0.222 kG/cm	defocusing
drift space	50.0	13.0	13.0				

Total length = 575.0 cm

to 90 MeV/c in the following manner. The first half of the system is tuned to focus the 75-MeV/c pions diverging from the source with finite size into a certain spatial image, with positive x-coordinate, which is blocked by one side of the asymmetric slit of the stopper.

Due to the dispersion effect the spot size and the position depend upon the momentum. However, it is shown that the image of the target in the higher momentum part is enlarged, but is pushed further toward the positive direction along the x-axis. The optical magnifications of the first half of our channel at a momentum of 75 MeV/c are -0.72 and -5.8 in the x- and y-direction, respectively.

Taking into consideration the image size of the 3.4 cm long target we choose the position of the outside edge of the asymmetric slit to be $W_{out} = 4.0$ cm, while the inside slit is fully open, i.e. $W_{in} = -13.0$ cm. The images of the low momentum pions are so wide at the position of the stopper that parts of them are not blocked. To reject these unblocked portions of low momentum pions the system is tuned to transform a parallel 82.5-MeV beam into a point at the exit point B. Then the major part of the low momentum pions will be blocked by the channel wall. The parameters for this tune are given in the seventh and eighth columns of Table II.

On the other hand, the spreading of the muons is expected to be broad enough so that some portion of the muon distribution will not be blocked by the slit, since the source points are vaguely distributed between the target and the channel entrance, as inferred from Table I.

In the calculation the linear approximation is adopted for the optics and only the first order is taken with respect to the dispersion of momentum in the dipole magnets. The effect of the fringing field at the edges of the dipole magnets is taken into account by replacing the angle of the pole face rotation β, for the vertical motion, by[14]

$$\beta - \frac{d}{\rho} \frac{1 + \sin^2 \beta}{\cos \beta}, \qquad (7)$$

where d is the half-gap size, ρ the radius of curvature.

The evaluated muon spectrum and average polarization of the output beam are given in Fig. 12. No pions are transmitted. The resultant muon

spectrum extends from a momentum of 67.5 MeV/c to 92.5 MeV/c, and its peak is at a momentum of 82.5 MeV/c. The polarization never differs much from 40 per cent.
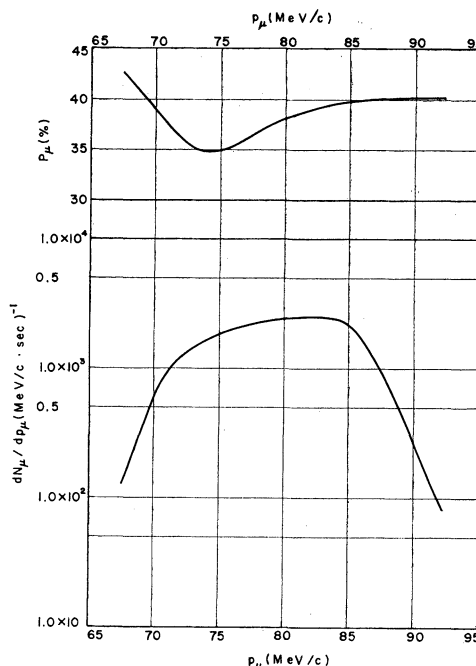

FIG. 12. Muon spectrum and average polarization of output beam.

The muon beam intensity and the corresponding average polarization are

$$N_\mu = 3.5 \times 10^4 \, \text{sec}^{-1},$$

and

$$\langle P_\mu \rangle = 37.8 \text{ per cent,}$$

respectively.

There are many possible ways of choosing the two central momenta of the system. A higher muon spectrum will be obtained, for example, by adjusting the first half of the channel to a central momentum of 100 MeV/c, and second half to a central momentum of 110 MeV/c. Then the accepted range of the momentum will be scaled by multiplying by the factor 4/3, while the height of the spectrum will be about 1.5 times as large as inferred from the curve in Fig. 7(a).

Let us consider another possible scheme to reduce the pion contamination at the exit. From the practical point of view some pion contamination may be allowable. Particularly for low momenta

the pion contamination is much reduced by the length of the channel. At $r = 100$ cm and $\delta = 0°$ the pi-mu ratio is minimum at a momentum between 60 MeV/c and 70 MeV/c. In the following consideration we suppose those values for r and δ. In order to focus the image of the target into a spatially small spot in one direction the bending plane is taken to be vertical, because the effective target size is smaller in this direction. Suppose that the system is tuned in the same way as for the previous horizontal channel, but the central momenta are 65 MeV/c in the first-half portion and 71.5 MeV/c in the second-half portion. Then the magnifications in the first-half portion at a momentum of 65 MeV/c are -1.0 in the x-direction (vertical), and -3.7 in the y-direction (horizontal).

The output muon and pion spectra are calculated with the assumption that the effective target width is 2.5 cm, and the width of a rectangular pion stopper placed at the center of the cross section at the midplane of the channel is 3.0 cm in the x-direction, and its length is the full size of the aperture in the y-direction (i.e. 26.0 cm).

The pion and muon beam intensities, and the corresponding average polarization are

$$N_\pi = 5.2 \times 10^4 \, \text{sec}^{-1},$$

$$N_\mu = 1.7 \times 10^4 \, \text{sec}^{-1},$$

and

$$\langle P_\mu \rangle = 34.9 \text{ per cent},$$

respectively.

The muon spectrum ranges from a momentum of 52.5 MeV/c to 77.5 MeV/c. On the other hand the pion spectrum is split into two parts, one of which is the low momentum part having momenta less than 65 MeV/c, and the other is the high momentum part having momenta greater than 77.5 MeV/c.

When the two bends are taken to be in the same direction, similar results are obtained.

The first order approximation is less reliable for large momentum dispersion. To confirm the validity of our conclusion of complete elimination of the pion contamination with our horizontal channel, the accepted pion flux is traced through the channel in a manner that takes account of the momentum difference exactly. The calculation†

† This calculation is done with the program PRPARE of S. Ohnuma.

shows that the pions with the momenta greater than 100 MeV/c are lost on the wall of the first-half portion of the channel. Some pions with the momenta less than 75 MeV/c are distributed broadly on the cross section at the position of the stopper, but are lost on the wall of the second-half portion. Pions with momenta between 75 MeV/c and 105 MeV/c are completely blocked by the stopper.

6. SUMMARY AND DISCUSSION

In the previous section the magnetic channels were studied for the transport of the muon clouds. The background pions are removed by making use of the fact that the source of pions (i.e. the target) is restricted to a well-defined spatial region, so that its image is well controlled by tuning the field strengths. But this holds only for a restricted momentum range, and some means should be provided to reduce the number of unwanted pions without much reducing the muon intensities if we wish to use a large momentum band. This is attained by taking a different central momentum for the tuning of the second portion. Since the source of the muons is distributed over a large spatial region between the entrance and the target, the phase-space distribution is broad. Because of this the muons are transmitted.

The polarization is not a consideration in this type of the channel, since the contributions from every decay are summed in order to get higher intensity.

The expected beam intensities for the horizontal channel, and for the vertical channels are comparable to those for stopped muon channels of the standard type.

One example of such a standard channel[8] gives the following usable pion-free muon spectra at its exit: for a central momentum tune of 90 MeV/c maximum spectrum from forward decay muons $dN_\mu/dp_\mu \sim 1 \times 10^4 \, (\text{MeV/c} \cdot \text{sec})^{-1}$ at $p_\mu = 115$ MeV/c, and another maximum from backward decay muons $0.3 \times 10^4 \, (\text{MeV/c} \cdot \text{sec})^{-1}$ at 50 MeV/c; and for the central momentum tune of 180 MeV/c the maximum spectrum from backward decay muons $1 \times 10^4 \, (\text{MeV/c} \cdot \text{sec})^{-1}$ at 110 MeV/c.

The lower momentum muons as obtained by our channel are more suited for stopped muon experiments because of the higher capture efficiency of low momentum muons.

The second-half of our channel is adjusted for a tune which transforms a parallel beam with a given larger central momentum into a spatial spot. But there will be room for improvement in tuning by optimizing the muon intensity.

In our two bend system pions enter the channel. Most of these disappear at the stopper and the rest hit the channel wall in the second portion. Therefore, some muons will be produced, with acceptable momenta from large angle decays. These contributions may change the beam intensity and the average polarization, but not substantially.

It is remarked that more muons will be transmitted if pion contamination is allowable to some extent. One such approach will be to make use of a very long channel with small δ, and to adjust it for low momentum muons.

To increase the channel acceptance it may be helpful to use gradient magnets, or a solenoid channel as part of the system. The gradient magnet will be effective also for the necessary bending.

The merits of our two-bend system are in its simplicity and versatility. In principle, the gradients of the quadrupole field and the gap sizes of the asymmetry slit are adjustable for any central momentum. Our channel can also be an achromatic, or monochromatic system simply by choosing appropriate tune. Therefore, it can be usable as the pion channel. And furthermore, it may be compatible with other channels which are set for the same target.

No calculations are carried out for the study of beam purity. However, a two-bend system will be quite effective in reducing the intensities of the neutral components (i.e. neutron and gamma ray) produced inside the target. The source of the electrons produced from the decays of π^0 is also located to the target. Therefore most of those electrons whose momenta are within the band characteristic to the channel will be removed along with the background pions. The electrons from the rare decay modes of pions form negligible contributions. The troublesome components will be secondarily produced from the inside wall of the channel by the scattering of pions and other particles.

REFERENCES

1. Meson Factories, Report of Ad Hoc Panel to the Office of Science and Technology (Chairman: H. A. Bethe), March 1964.
2. *Proposal for a High-Flux Meson Facility*, Los Alamos Scientific Laboratory, September 1964.
3. *Design of a Very High Intensity Proton Linear Accelerator as a Meson Factory*, Yale Report, Y-12, Yale University, October 1964.
4. A. Citron, M. Morpurgo, and H. Øveras, *The High Intensity Muon Beam with Low Pion Contamination at the CERN Synchrocyclotron*, Report CERN 63–35, November 27, 1963.
5. G. Culligan, et al., *Proc. Conference on High Energy Cyclotron Improvement, College of William and Mary, 1964*, p. 237. G. Culligan et al., ibid., p. 264.
6. H. O. Funsten and R. T. Siegel, 'Meson Channel Design for SREL Synchrotron', *IEEE Trans., Nucl. Sci.*, NS-16, No. 3, 508 (1969).
7. *Dubna muon channel*, No details are available.
8. V. W. Hughes, S. Ohnuma, K. Tanabe, and H. Vogel, 'Stopped Muon Channel—Design Status—', Report for the Second LAMPF Users Meeting, Los Alamos Scientific Laboratory, January 1969. V. W. Hughes, S. Ohnuma, K. Tanabe, and H. Vogel, 'Stopped Muon Channel for LAMPF', Los Alamos Scientific Laboratory Report, July 1970, to be published.
9. Nevis Laboratory, Columbia University, private communications.
10. L. Lederman and J. Rainwater, private communication.
11. D. Theriot, private communication (July 1969) on the experiment done by the group of Los Alamos Scientific Laboratory at Lawrence Radiation Laboratory.
12. E. Heer, et al., *The Production of Charged Pions by 600 MeV Protons on Various Nuclei*, Intermediate Energy Physics (Williamsburg Conference, February 1966), p. 277.
13. A. Citron, J. Fronteau, and J. Hornsby, *Calcul Automatique des Faisceaux de π et des Faisceaux de μ Programme Fortran*, Report CERN 63–30, August 30, 1963.
14. H. A. Enge, Sec. 4.2.3 *Focusing of Charged Particles*, Vol. II, ed. by A. Septier, Academic Press, New York (1967).